Applied Catalysis A: General 527 (2016) 161–170

Contents lists available at ScienceDirect

Applied Catalysis A: General

journal homepage: www.elsevier.com/locate/apcata

Hydrogen production from catalytic steam reforming of phenol with bimetallic nickel-cobalt catalyst on various supports

Walid Nabgan[a,b], Tuan Amran Tuan Abdullah[a,b,*], Ramli Mat[b], Bahador Nabgan[a,b], Sugeng Triwahyono[c], Adnan Ripin[a]

[a] Centre of Hydrogen Energy, Institute of Future Energy, Universiti Teknologi Malaysia, UTM Skudai, 81310 Johor, Malaysia
[b] Department of Chemical Engineering, Faculty of Chemical & Energy Engineering, Universiti Teknologi Malaysia, UTM Skudai, 81310 Johor, Malaysia
[c] Centre for Sustainable Nanomaterials (CSNano), Department of Chemistry, Universiti Teknologi Malaysia, UTM Skudai, 81310 Johor, Malaysia

ARTICLE INFO

Article history:
Received 3 July 2016
Received in revised form 28 August 2016
Accepted 31 August 2016
Available online 13 September 2016

Keywords:
Hydrogen production
Steam reforming
Phenol
Bimetallic nickel-cobalt
Various supports

ABSTRACT

Catalytic phenol steam reforming with the aim of hydrogen production was studied in terms of bimetallic nickel-cobalt supported by CeO_2, ZrO_2, La_2O_3, γ-Al_2O_3, and α-Al_2O_3. The catalysts (each formed of 5% wt. of nickel and 5% wt. of cobalt on the support) were prepared according to the impregnation method. The effect of different supports on the properties and catalytic behaviour with the aim of hydrogen production, phenol conversion, and coke formation on the surface of the catalysts were studied. The physical and chemical properties of the catalysts were characterised in terms of their surface area, acidity, basicity, reducibility, crystallinity, and coke formation (for spent catalysts). The catalysts were tested by using a micro-reactor fixed bed at a temperature range of 500–800 °C. The activity of the catalysts on phenol conversion and hydrogen yield depends on the basic and acidic site of the catalysts as well as the metal interaction with the support. Results of various experiments in catalytic activity confirmed that a higher production of H_2 occurred in the presence of high CO_2 uptake and H_2 consumption which are characterised by basicity and reducibility analysis respectively. The coke analysis results show that the irreducible oxides for the Ni-Co bimetallic catalyst are more favour for coke formation than reducible oxides. All catalysts were active in the reformative reactions but the catalysts supported on the reducible oxides of ZrO_2 showed superiority in activity and stability. The most active catalyst was Ni-Co/ZrO_2 because of having the tetragonal phase structure which is favour in reforming processes, strong metal-support interaction, high surface area, the lowest coke formation, and six days' reformative stability. The catalyst test shows that the phenol conversion achieved at 650 °C is 75.9% and hydrogen yield is 80.7% for Ni-Co/ZrO_2 catalyst. The reaction rate and activation energy with respect to Ni-Co/ZrO_2 catalyst were found to be 11.17 mmol/g s and 102.41 (J/mol), respectively.

1. Introduction

Hydrogen can be considered an attractive source of carrying energy due to the advanced development of proton exchange membrane fuel cell (PEMFC), a green technology. PEMFC is well-known to be a clean technology for mobile application (such as transportation) and aims to replace fossil fuel combustion engines. Since hydrogen does not exist naturally or is stable in its normal condition, it must be extracted from a renewable source, compound or molecules that contain hydrogen [1]. Phenol, with six hydrogen atoms, six carbon atoms, and an oxygen atom, is considered to contain a high level of hydrogen. Interestingly, phenol can be obtained from a side reaction during the pyrolysis of biomass. Phenolic compounds are the main bio-oil components with up to 38% wt. [2,3]. Phenol was further recognized as the main component of tar formed following wood-biomass gasification by steam in a fluidized bed reactor in the low temperature range (600–700 °C) [4–6]. According to the previous research [7], there are two successive reactions that may take place in the steam reforming of phenol. Phenol steam reforming reaction and water gas shift reaction are represented by Eqs. ((1) and (2)).

$$C_6H_5OH + 5H_2O \rightarrow 6CO + 8H_2 \quad \Delta H^o = 710.91 kJ/mol \tag{1}$$

$$CO + H_2O \leftrightarrow CO_2 + H_2 \quad \Delta H^o = -41.15 kJ/mol \tag{2}$$

* Corresponding author at: Hydrogen and Fuel Cell Lab, N29, Universiti Teknologi Malaysia, Skudai, 81310, Malaysia.
E-mail addresses: tamran@cheme.utm.my, tuanamran@utm.my (T.A. Tuan Abdullah).

http://dx.doi.org/10.1016/j.apcata.2016.08.033
0926-860X/

However, one of the major problems in the phenol steam reforming is the high potential formation for some by-products such as carbon [7–9]. This carbon formation will lead to catalyst deactivation and can make troubles for continuous steam reforming process and sustainable production of hydrogen.

The reaction product of biomass pyrolysis typically contains a high molecular weight of hydrocarbon, phenolic compounds, acid, and water. It can directly convert to highly valuable gas hydrogen via catalytic steam reforming. It has been found that steam reforming is the most effective and convenient method for hydrogen production from hydrocarbons compared to other methods such as auto-thermal reformation, partial oxidation, and dry reformation [10,11].

Many typical active metals such as Ni [8], Rh [12,13], Fe [7], Rh-Fe [6], CaO [14], Pt, Pd, and Rh [15] over irreducible oxide supports such as γ-Al_2O_3 [15,16], La_2O_3 [8,13,16,17] and reducible oxide supports such as ZrO_2 [6,8,12,13,15], MgO [6,7,12], and CeO_2 [6–8,12,13,15] have been studied in terms of phenol reformation. For example, Matas Güell, et al. [8] found that Ni/K-La_2O_3-ZrO_2 and Ni/CeO_2-ZrO_2 catalysts exhibited high activity and good stability in phenol conversion. However, the catalysts suffered in deactivation due to coke formation. Ruthenium (Rh) supported on different composition of CeO_2, ZrO_2 and La_2O_3 was examined by Constantinou, et al. [13] at a steam to phenol ratio of 67:1. They achieved 80% phenol conversion and 80% hydrogen yield at a low temperature of 450 °C for 5 wt.% Rh supported on 13 wt% Ce, 83 wt% Zr and 4 wt% La catalyst. This shows good performance, but there are drawbacks due to the high price of Ru itself as a precious metal. In general, ZrO_2 exists in three different polymorphs at ambient pressures: monoclinic (m-ZrO_2), tetragonal (t-ZrO_2), and cubic (c-ZrO_2). The t-ZrO_2 phase shows higher stability, performance and metal dispersion for chemical reactions [18–20]. Another important work is that of Polychronopoulou et al. [7], who examined Fe supported on MgO-Al_2O_3 and MgO-CeO at temperature between 600 and 700 °C and a water to phenol ratio of 8:1. They found that a 5 wt.% Fe/50MgO-50CeO catalyst is more active in terms of H_2 production and has low coke formation on its surface. It is believed that Al_2O_3 was the main contribution to coke formation and suffered less activity compared to a catalyst supported on MgO-CeO. Other works applied La_2O_3 support catalysts for phenol [8,13,16], acetic acid [21,22], and ethanol [23,24] reformation. It was found that applying a La_2O_3 support in the catalyst highly affected the water gas shift reaction and increased H_2 production.

Among the metals, nickel as an active metal has been selected due to its considerably cheaper price compared with precious metals (for example, platinum, rhodium, or ruthenium) at high catalytic activity in terms of the cracking of C—C and C—H bonds [25]. In previous research, in the steam reforming of acetic acid [26,27] and ethanol [28,29], a basic catalyst was found to be highly active in fuel conversion and had good selectivity in terms of hydrogen yield. Cobalt can assist C—C bond cleaving at temperatures as low as 400 °C and this shows high production of H_2 and CO_2 [28]; this is due to the highly favourable water gas shift reaction [10,29,30]. In our previous researches [31,32] we found that the same combination of Ni and Co metals may improve the performance of the catalyst in the acetic acid steam reforming reaction. Zhang, et al. [33] examined the effect of bimetallic Ni-Co for the CO_2 reformation of methane. They found that bimetallic Ni-Co catalysts exhibit highly stable activity with no deactivation and no detectable carbon formation. De Sousa et al. [34] also investigated bimetallic nickel-cobalt catalysts for methane dry reformation. They also reported that a different catalytic support will have an effect on the catalyst's performance. They found that the NiCo dispersed on $NiAl_2O_4$ species was highly active in terms of CH_4 conversion. $NiAl_2O_4$ species was highly active in terms of CH_4 conversion, whereas Ni° dispersed on either Fe_3O_4—Co_3O_4 or CeO_2—$NiAl_2O_4$ provided lower catalytic performance due to active phase degradation.

According to the above-mentioned information, there have not been systematic studies about the effect of the support on hydrogen production from phenol steam reforming over supported bimetallic Ni-Co catalysts. However, different type of support can have a significant effect on catalytic activity and selectivity toward phenol steam reforming reaction. The metal-support interactions can have a significant effect on catalytic activity and selectivity in phenol steam reforming reaction. Another point is that oxygen mobility of the support is a critical property to favour carbon removal and avoid deactivation. However, during reaction, the morphology and the oxidation state of the metal particles are changed and the actual dispersion under reaction conditions cannot be represented by initial dispersion of the metal catalyst. Therefore, the study of the effect of reducible oxides such as ZrO_2 and CeO_2 and irreducible oxides such as La_2O_3, γ-Al_2O_3, and α-Al_2O_3 supports on the performance of bimetallic Ni—Co catalysts with the aim of hydrogen production from phenol steam reforming is of considerable interest. The overall performance of these supports for bimetallic Ni-Co catalyst will be calculated based on phenol conversion and the hydrogen yield. Thus, the physicochemical properties and activity of bimetallic Ni—Co catalyst in relation to La_2O_3, ZrO_2, CeO_2, γ-Al_2O_3, and α-Al_2O_3 supports in the steam reforming of phenol with the aim of hydrogen production is reported herewith. In addition, the activation energy (Ea) and the reaction rate for phenol conversion for every catalyst were carried out.

2. Experimental procedure

2.1. Catalyst preparation

The bimetallic catalysts of 5 wt.% Ni and 5 wt.% Co supported on La_2O_3, ZrO_2, CeO_2, α-Al_2O_3, and γ-Al_2O_3 (all from Sigma-Aldrich) were prepared by using the impregnation method. Previous researched [35–37] were reported that the 5 wt.% Ni in the bimetallic catalysts show high activity in the reforming reaction. The catalysts were prepared by mixing nickel nitrate hexahydrate and cobalt nitrate hexahydrate AR with a metal oxide support in deionised water based on their metal content. This mixture was continuously stirred on a hotplate at 90 °C until it becomes slurry. The slurry was dried in an oven at 110 °C overnight, followed by calcination at 750 °C overnight. The powder catalyst will pass the reactor mesh; therefore, the catalyst's particle size was required to be 1 mm in order that it could hold in the reactor. Thus, the calcined catalyst was crushed and filtered on two layers of 35 mesh and 34 mesh sieves to obtain a particle size of 1.0 to 1.4 mm.

2.2. Catalyst characterisation

A chemisorption analyser, Micromeritics Chemisorb 2720, was used to evaluate the reducibility of the bimetallic catalysts on the support by applying a temperature-programmed reduction of hydrogen (TPR-H_2) method. 25 mg of the catalysts were treated at 300 °C for an hour under a high purity of 20 mL/min helium (99.99%) to remove moisture and other adsorbate impurities. The TPR-H_2 profile was obtained by ramping the temperature at 10 °C/min under 20 mL/min of 10% (vol.) H_2 in argon.

The same apparatus of chemisorption was used to carry out the temperature-programmed desorption of CO_2 and NH_3 to evaluate the basicity and acidity, respectively. 35 mg of the sample was kept under a 30 mL/min argon flow rate at 600 °C for 60 min, then cooled down to 25 °C and kept under a 20 mL/min helium flow rate for 30 min. The CO_2 saturation of the catalyst was carried out for 30 min at 20 mL/min under purified CO_2. The heating rate was set

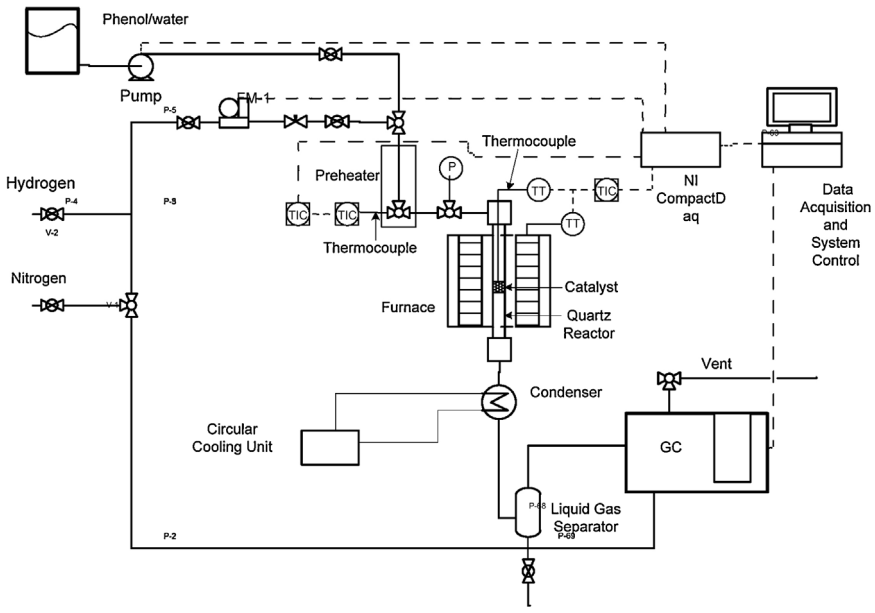

Fig. 1. Experimental rig setup of fixed bed reactor for phenol steam reforming.

at 10 °C/min from 50 to 800 °C. A similar method was applied for TPD-NH_3, except that the adsorbate gas was 5% (vol.) NH_3 in argon.

The crystalline structure of the reduced catalysts was determined by x-ray diffraction (XRD) (High Resolution X-Ray Diffractometer Bruker D8 Advance) using Cu Kα radiation at 40 kV and 30 mA, with a scanning angle (2θ) of 4 to 90°. Prior to analysis, all samples were reduced with 30 mL/min of purified hydrogen at 600 °C for an hour and then cooled to room temperature under a nitrogen flow.

The multipoint BET-N_2 method was used to measure the total surface area of the catalyst using a Micromeritics Gemini 2360 Surface Analyzer. The pressure ratio of P/Po was measured from 0.05 to 0.3 with five points.

In order to evaluate the carbon deposition on the catalyst after the reaction in the spent catalyst, thermo-gravimetric analysis (TGA) was carried out using the Perkin Elmer TGA (4000), operated under a flow of nitrogen at a heating rate of 10 °C/min and at the temperature range of 30 to 950 °C. The methodology was based on coking studies and is similar to the previous work [31,32,38–40]. According to the previous investigations [41,42], there is no difference between use of nitrogen or air in the total weight loss (material decomposition) but nitrogen increase the coke decomposition temperature

2.3. Activity test

The tests were performed using 0.2 g of the catalyst diluted with 0.3 g silicon carbide, SiC (due to its behaviour of enhancing catalyst activity [36,43–45] and can significantly reduce the overall cost of the catalyst [46]) in a micro fixed bed reactor as illustrated in Fig. 1. The catalyst was placed in a 0.5 inch outside diameter (OD) quartz tube with the end tip of thermocouple type K touching the bed. Prior to reaction, the catalyst was purged with nitrogen at 300 °C with 30 mL/min for 30 min, followed by in-situ reduction at 600 °C for one hour under 30 mL/min of pure hydrogen. In our previous research [31,32,38], we found that at 600 °C the complete reduction of both nickel oxide (NiO) and cobalt oxide (CoO) to metallic Ni and metallic Co was achieved. The mixture of phenol and water ((H_2O/phenol(mol/mol) = 9:1) was fed by a HPLC pump (Bio-Rad™, Series 1350) with the flow rate of 0.36 mL/min, and then it was mixed with a carrier gas of N_2 at 30 mL/min and passed through the pre-heater before entering the reactor in the furnace. The steam to phenol mole ratio of 9:1 and 30 mL/min of nitrogen as carrier gas were used for all of the experiments. Temperatures between 500 and 800 °C were employed for six hours in each experiment. The gas products were analysed using an on-line gas chromatography (GC) equipped with a thermal conductivity detector (TCD) (Agilent 6890N) and installed with a 30 m × 0.53 mm Carboxen Plot 1010 capillary column (Supelco®). Meanwhile, the liquid product was analysed using a GC-FID (HP 5890 Series II) and a 0.53 mm × 30 m Db-Wax capillary column. The 95% confidence level interval was used to calculate the experimental uncertainty in the conversion and the gas product distribution.

Eqs. (3) and (4) were applied to compute the phenol conversion and the product (X: H_2 (or) CO (or) CO_2) yield. In Eq. (3), $[F]_{in}$ is the total molar flow rate of the feed, and $[F]_{out}$ is the total molar flow rate at the exit of the reactor.

$$\text{Conversion}\,(\%) = \frac{[F]_{in} - [F]_{out}}{[F]_{in}} \times 100\% \quad (3)$$

$$\text{Xyield}\,(\%) = \frac{\text{moles of X obtained}}{\text{moles of X obtained from stochiometric potential}} \times 100 \quad (4)$$

3. Results and discussion

3.1. Catalyst characterisation

The XRD patterns of the Ni-Co catalyst in terms of different supports after reduction at 600 °C are presented in Fig. 2 with the reference peaks from JCPDS. The characteristic diffraction peaks of metallic Ni^o (111) [JCPDS 45-1258] and Co^o (111) [JCPDS 01-1254] are located at 2θ = 44.4° [31,32,47] and are hard to distinguish from each other due to their similar morphology and characteristic peaks [48]. For all catalysts, no NiO or CoO peaks were detected. This is probably due to the complete or partial reduction of NiO and CoO to metallic Ni^o [49,50] and metallic Co^o [51], respectively.

The XRD patterns of Ni-Co/La_2O_3 [JCPDS 02-0688 [52,53]] showed peaks at 2θ = 27.28, 27.93, 31.47, 39.52, 47.07, 48.63, 50.12, 55.36, and 64.04 representing the (1 1 1), (1 1 1), (2 0 0), (2 1 1), (2 2

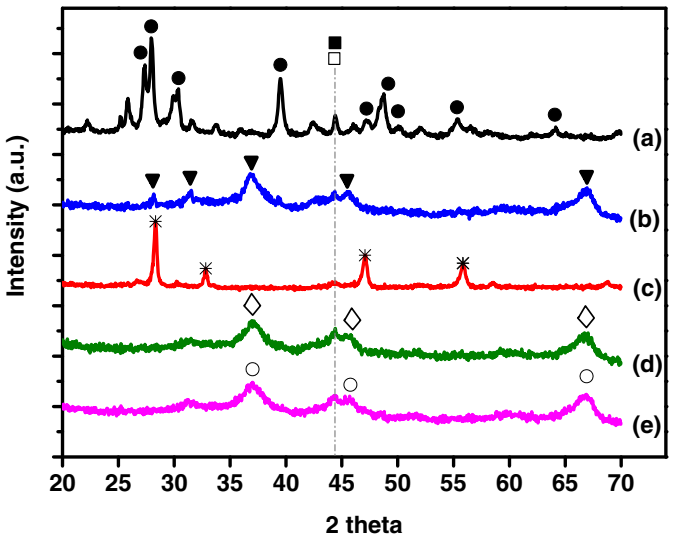

Fig. 2. XRD patterns for fresh-reduced catalysts at 600 °C, (a) Ni-Co/La_2O_3, (b) Ni-Co/ZrO_2, (c) Ni-Co/CeO_2, (d) Ni-Co/α-Al_2O_3 and (e) Ni-Co/γ-Al_2O_3 catalysts. (■) peaks correspond to Ni°, (□) peaks correspond to Co°, (∗) peaks correspond to CeO_2, (○) peaks correspond to γ-Al_2O_3, (◊) peaks correspond to α-Al_2O_3, (▼) peaks correspond to ZrO_2 and (●) peaks correspond to La_2O_3.

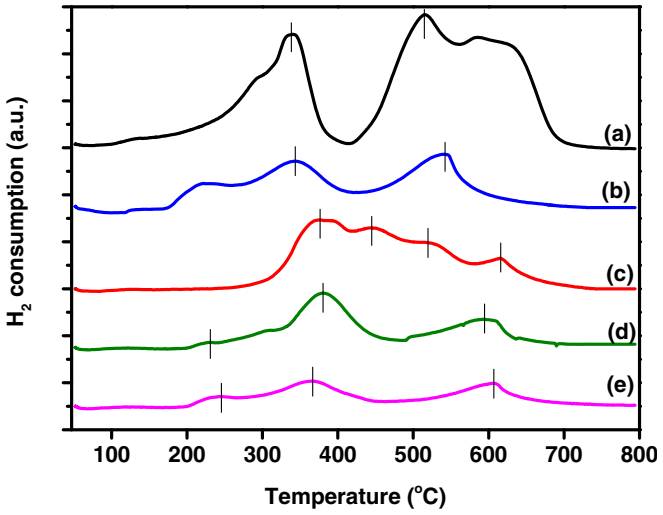

Fig. 3. Temperature-programmed reduction profiles of 10% vol of 10% vol H_2/Ar, heating rate 10 °C/min for (a) Ni-Co/La_2O_3, (b) Ni-Co/ZrO_2, (c) Ni-Co/CeO_2, (d) Ni-Co/α-Al_2O_3 and (e) Ni-Co/γ-Al_2O_3 catalysts.

0), (2 2 1), (2 2 1), (3 1 1), and (4 0 0) crystal plane of hexagonal phase respectively [53,54]. The additional peaks for the Ni-Co/La_2O_3 catalyst signal might be indexed to the $NiLaO_3$ phase which can be attributed to the strong interaction between Ni active metal and La_2O_3 support. Cubic perovskite-type of $NiLaO_3$ phase [JCPDS 33-0710 [55,56]] were observed for Ni-Co/La_2O_3 catalysts at 2θ = 40.67 and 51.93 representing the (2 1 1) and (3 1 0) crystal plane, respectively. The XRD patterns of Ni-Co/ZrO_2 catalyst resulted in a number of peaks located at 2θ of 28.17, 36.78, 39.29, 45.59, and 66.94° corresponding to (200), (211), (220), (311), and (421) crystal planes, which can be attributed to the monoclinic [JCPDS 83-0936] structure of ZrO_2 and this reflects Tarak, et al.'s work [57]. The tetragonal ZrO_2 [JCPDS 83-0943] phases are identified at 2θ = 31.53° corresponding to (210) crystal plane and by comparison with those reported in references [19,58]. The tetragonal phase structure of ZrO_2 is more desirable than monoclinic structure in the reforming process [59]. The XRD peaks observed at 2θ of 28.33, 32.82, 47.08, and 55.82° were respectively indexed as (111), (200), (220), and (311) planes of the fluorite structure (JCPDS 81-0792) of CeO_2. The same results were reported previously [60,61]. However, the XRD patterns of the reduced catalysts showed diffraction peaks at approximately 2θ = 37.04, 45.75, and 66.71° corresponding to (111), (200), and (220) planes related to α-Al_2O_3 [JCPDS 83-2080] [62] and γ-Al_2O_3 [JCPDS 86-1410] crystalline structure [62,63].

The surface area of all catalysts has been measured by the Brunauer-Emmett-Teller (BET) technique. Table 1 shows the BET surface area of the Ni—Co supported on La_2O_3, ZrO_2, CeO_2, γ-Al_2O_3, and α–Al_2O_3. The catalysts were calcined at 750 °C and reduced at 600 °C. The specific surface areas of five spent catalysts were also determined by nitrogen adsorption in order to evaluate if coking is one of the possible reasons for catalyst deactivation. For these catalysts, the BET result shows that their surface areas are about 9–95m^2/g for the fresh (after calcination) and 7–67 m^2/g for the spent catalysts (after steam reforming reaction). The decrease in surface area of catalysts after reaction is mainly due to coke deposition on the surface and to some extent within the pores of the catalyst [64]. The surface areas of these catalysts are in the following order: Ni-Co/γ-Al_2O_3 > Ni-Co/α-Al_2O_3 > Ni-Co/ZrO_2 » Ni-Co/La_2O_3 > Ni-Co/CeO_2. The lower surface area corresponds to a relatively lesser number of active sites [65]. It was found that the specific surface area of the Ni—Co supported on La_2O_3, ZrO_2, CeO_2, γ-Al_2O_3, and α–Al_2O_3 decreased after reaction by 32%, 21%, 24%, 24%, and 30%, respectively.

The reducibility properties of bimetallic Ni-Co catalysts were investigated using the H_2-TPR technique. H_2 consumption, as a function of temperature, is shown in graphs in Fig. 3 and H_2 consumption data is summarised in Table 1. In Fig. 3 and Table 1, TPR-H_2 shows that the reducibility of Ni-Co species, in the temperature range of 50 to 800 °C, increases in the following order: Ni-Co/La_2O_3 > Ni-Co/CeO_2 > Ni-Co/ZrO_2 > Ni-Co/α-Al_2O_3 > Ni-Co/γ-Al_2O_3. Previous research [66,67] has shown that the reduction peaks before 500 °C illustrate the reduction of nickel and cobalt ions to metallic Ni° and Co°, which can also be confirmed by XRD analysis. The Ni-Co/La_2O_3 catalyst shows twin peaks in the initial part of the reduction of Co species at temperatures between 250 and 420 °C and twin peaks in terms of the signal for the reduction of Ni species at temperatures between 420 and 700 °C. A less intense peak is seen at 290 °C and is due to the reduction of Co species that are in weak interaction with the support. The higher temperature peak at 341 °C may be because of a strong interaction between Co and the La_2O_3 support. The two distinctive reduction peaks in the temperature range of 410 to 700 °C are due to the strong and weak interaction of Ni with La_2O_3.

The TPR signal for the ZrO_2-supported catalyst shows the three reduction peaks at 228 °C, 342 °C, and 521 °C. Previous researches [68,69] reported that the peak around 340 °C defines the reduction of Ni^{2+} to Ni°. Strong interaction of the present bimetallic Ni-Co with ZrO_2 is also supported by the broadening peak for the high surface area samples (63.7 m^2/g). This signal shows only one peak at 541 °C regarding the strong interaction between the Ni species and the ZrO_2 surface [70]. This peak is the same as in previous research, which detected the reduction of Ni/$CeZrO_2$ [71]. For La_2O_3 and ZrO_2-supported catalysts, the signal is shifted to lower temperatures of 341 °C and 516 °C for La_2O_3 and 342 °C and 541 °C for ZrO_2 supports. This might be because of the presence of Co and Ni species and the low strength of interaction between the La_2O_3 and ZrO_2 supports compared to CeO_2, α-Al_2O_3, and γ-Al_2O_3 [72]. The ceria-supported Ni-Co exhibited a large single reduction peak which is the second highest level of H_2 consumption. The broad feature peaked at ~610 °C corresponding to the reduction of the surface ceria [73]. At low temperatures (between 300 °C and 400 °C) NiO to Ni reduction processes take place [74] while 442 °C can be attributed to the reduction of NiO species with higher inter-

Table 1
Surface area, basicity, reducibility and acidity data of catalysts.

Catalyst	Ni (wt.%)[a]	Co (wt.%)[a]	Fresh catalyst surface (m^2/g)	Spent catalyst surface (m^2/g)	CO_2 uptake (μmol/g)	H_2—Consumption (mmol/g)	NH_3 uptake (μmol/g)
Ni-Co/La_2O_3	4.97	4.98	17.3	11.8	401	2.134	413
Ni-Co/ZrO_2	4.98	4.99	63.7	50.4	25	1.514	650
Ni-Co/CeO_2	4.96	4.97	9.7	7.4	41	2.001	208
Ni-Co/α-Al_2O_3	4.97	4.95	71.9	54.8	16	1.075	785
Ni-Co/γ-Al_2O_3	4.98	4.97	95.8	67.3	700	0.916	630

[a] The metal content was measured by ICP test.

action with the support [73]. There are low temperature reduction peaks for α-Al_2O_3 and γ-Al_2O_3 at 230 °C and 242 °C respectively, which are generally due to the weak interaction between the Ni-Co bimetallic catalyst and the supports [75]. The high temperature peak at 592 °C for α-Al_2O_3 might be due to the facilitation by Ni of Co reduction. This suggests that the 380 °C and 592 °C peaks correspond to the interaction between the bimetallic Ni-Co phase and the α-Al_2O_3 support. A nearly exact result was found previously regarding the reducibility properties of a α-Al_2O_3 support with a bimetallic Re-Co catalyst [76]. The maximum reduction peak in terms of the γ-Al_2O_3 support occurred at 370 °C and 607 °C. Moreover, the peak at 370 °C, which belongs to the interaction of the Co species with γ- Al_2O_3, was broad and not well-defined. The difference in the reducibility of the La_2O_3, ZrO_2, CeO_2, γ-Al_2O_3, and α–Al_2O_3-supported Ni-Co metal is due to differences in the properties of the supports. This different reducibility and metal to support the interaction is one of the determinants of a water gas shift reaction in terms of the performance of catalytic activity.

The chemisorption and dissociation of CO_2 can be improved through enhancement of catalyst basicity, which is usually determined by the CO_2-TPD technique. All samples were pre-treated by calcination at 750 °C in air overnight, followed by a reduction at 600 °C in H_2 gas for one hour. The low temperature desorption peaks (below 400 °C) could be attributed to weak interaction between CO_2 molecules and weak basic sites on the catalyst surface, whereas the CO_2 desorption peaks between 400 °C and 700 °C can be attributed to a medium basic site and the CO_2 desorption peaks above 700 °C represent a strong basic site [77]. Fig. 4 illustrates the basicity of the catalysts analysed by TPD-CO_2 and the number of base sites were estimated based on the area under their TPD curves for the temperature range as summarised in Table 1. In general, temperature represents base strength, and peak area represents the base amount of the catalyst. There is a low base strength and base amount for the detection of Ni-Co/ZrO_2, Ni-Co/CeO_2, and Ni-Co/α-Al_2O_3. This is due to the weak basicity of these three catalysts. Some previous studies found that ZrO_2 [78,79], CeO_2 [80,81], and α–Al_2O_3 [82] supports have OH—(hydroxyl) groups in their structure. Therefore, the weak basic sites for these three supports might be due to the formation of hydrogen carbonates that results from the interaction of CO_2 with the weak basicity of OH—groups [83]. The hydroxyl group is mainly formed due to the coordination of metals during the preparation of the catalyst. The TPD-CO_2 desorption curve of Ni-Co/La_2O_3 displayed three desorption peaks at 408 °C, 540 °C, and 738 °C, which can be attributed to low (bicarbonate), medium (bidentate carbonate), and high (unidentate carbonate) strength. This is in agreement with results reported in existent literature regarding the basicity of Ni-based catalysts [84]. The highly preferential adsorption of CO_2 on the La_2O_3 surface is in agreement with the previous research of Liuye, et al. [85]. It is obvious that, in a Ni-Co/γ-Al_2O_3 sample, a weak basic site appears at 131 °C and, at temperatures higher than 400 °C, the peak disappears. The same result was obtained for Ni-K/Al_2O_3 in the research of Ching, et al. [86]. They showed that the disappearance of the TPD-CO_2 signal at high temperatures is because K species might cover the site that strongly adsorbed CO_2.

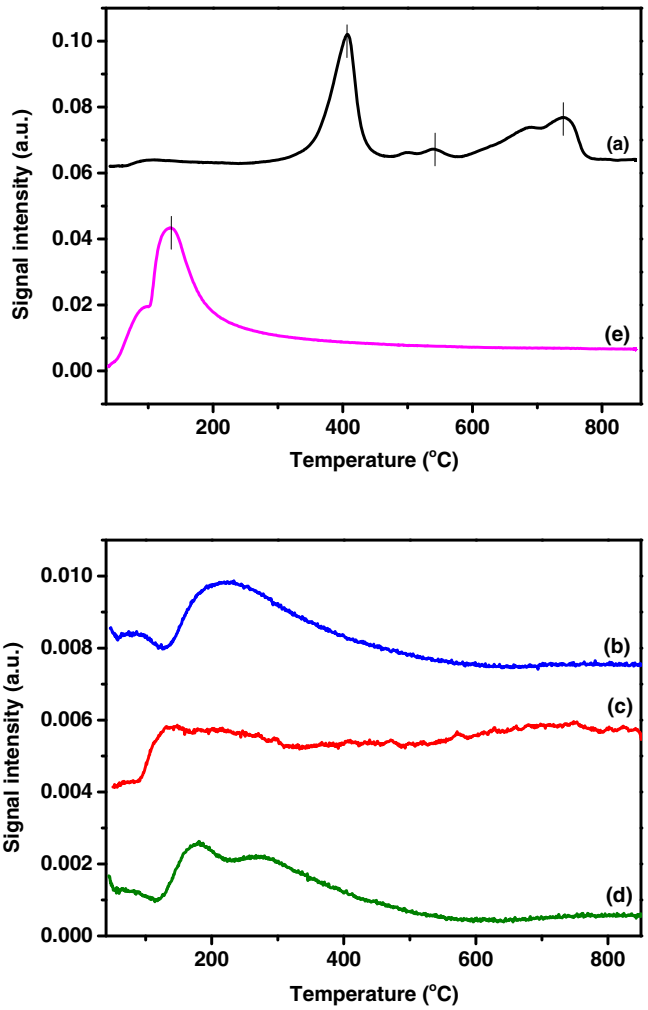

Fig. 4. Temperature-programmed desorption profiles of CO_2 for (a) Ni-Co/La_2O_3, (b) Ni-Co/ZrO_2, (c) Ni-Co/CeO_2, (d) Ni-Co/α-Al_2O_3 and (e) Ni-Co/γ-Al_2O_3 catalysts.

The NH_3-TPD results of the bimetallic Ni-Co catalysts are shown in Fig. 5. The total surface acid amounts (defined as desorbed NH_3) are shown in Table 1. The acid site distributions are mainly classified by temperature range as weak (<250 °C), medium (250–400 °C), and strong (>400 °C) acidic sites [87]. Fig. 5 indicates two peaks in different positions except in the case of the Ni-Co/La_2O_3 sample, in which one peak appeared at 220 °C. This shows there are weak acidic sites. For the catalyst supported by CeO_2, ZrO_2, γ-Al_2O_3, and α-Al_2O_3, the first peaks were at a temperature of 100 °C, while the second peaks were at 790 °C. The presence of these weak acidic sites might be related to centres created by the incorporation of the metal [88]. A qualitative comparison of the peak intensities shown in Table 1 illustrates that the α-Al_2O_3-supported catalyst adsorb more ammonia, followed by ZrO_2, γ-Al_2O_3, La_2O_3, and CeO_2 supports (from high to low capacity of ammonia uptake) and hence a low

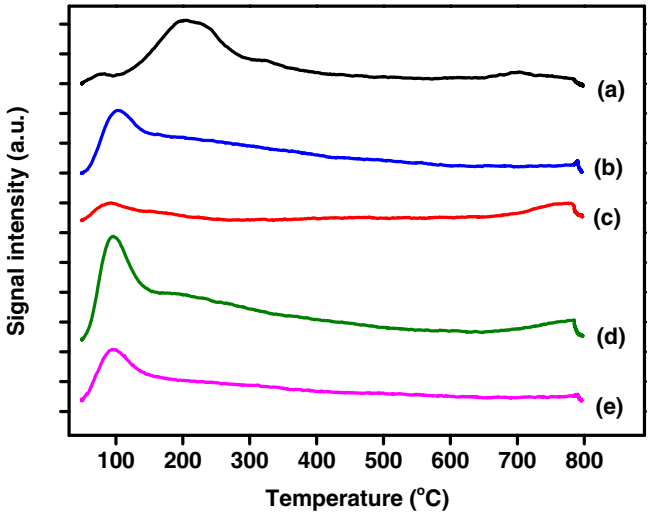

Fig. 5. Temperature-programmed desorption profiles of NH_3 for (a) Ni-Co/La_2O_3, (b) Ni-Co/ZrO_2, (c) Ni-Co/CeO_2, (d) Ni-Co/α-Al_2O_3 and (e) Ni-Co/γ-Al_2O_3 catalysts.

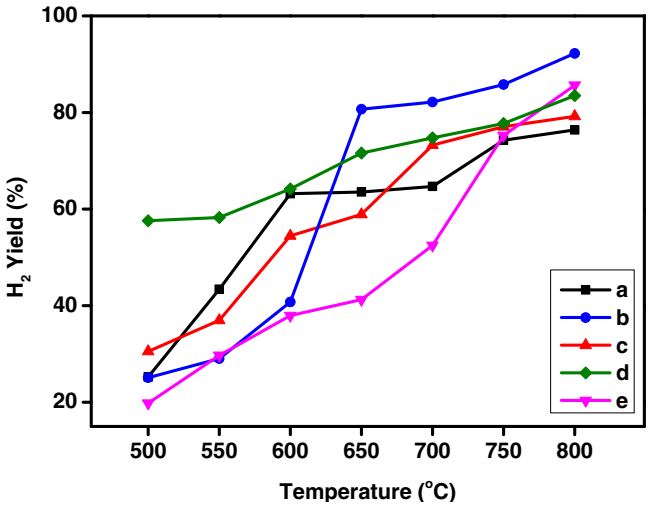

Fig. 7. Hydrogen yield at 500 to 800 °C for (a) Ni-Co/La_2O_3, (b) Ni-Co/ZrO_2, (c) Ni-Co/CeO_2, (d) Ni-Co/α-Al_2O_3 and (e) Ni-Co/γ-Al_2O_3 catalysts.

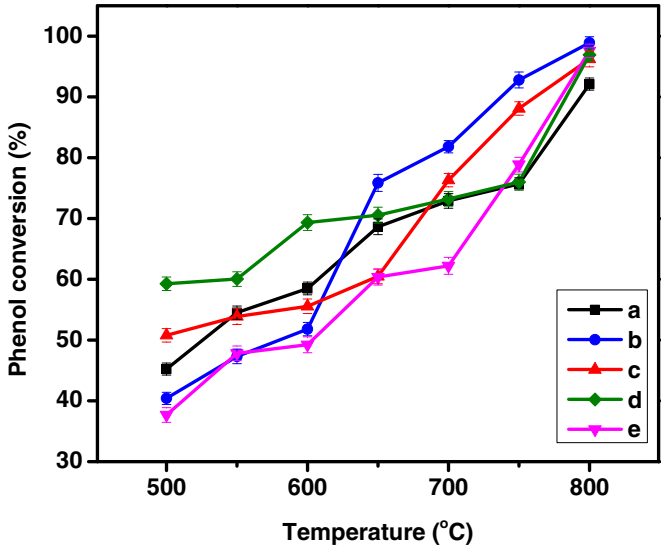

Fig. 6. Effect of temperature on phenol conversion [error bars equal 95% confidence interval (CI)] for (a) Ni-Co/La_2O_3, (b) Ni-Co/ZrO_2, (c) Ni-Co/CeO_2, (d) Ni-Co/α-Al_2O_3 and (e) Ni-Co/γ-Al_2O_3 catalysts.

concentration of acidic sites on the surface. These additional features indicate that there are different acidic sites which can adsorb ammonia with varying strengths. The presence of a high temperature feature around 790 °C in terms of Ni-Co/α-Al_2O_3 followed by Ni-Co/ZrO_2 is especially indicative of stronger acidic sites.

3.2. Catalyst performance test

The activity of bimetallic Ni-Co catalysts supported on reducible oxides of ZrO_2 and CeO_2, and irreducible oxides of La_2O_3, γ–Al_2O_3 and α–Al_2O_3 were firstly tested in terms of phenol steam reforming in the temperature range of 500 °C to 800 °C. The influence of reaction temperature on phenol conversion steam reforming is shown in Fig. 6. In general, the reformative activity of phenol conversion increases as the temperature increases. This is because of favourable hydrocarbon conversion at high temperatures [89]. Previous works have achieved the same result of increasing phenol conversion activity with high temperatures [7,90]. As seen in Fig. 6, the highest phenol conversion was achieved for the Ni-Co/ZrO_2 catalyst. For this catalyst, the conversion increased from 75.9% at 650 °C to 98.9% at 800 °C. This high activity of reducible ZrO_2 oxide support for bimetallic Ni-Co catalyst might be due to strong metal-support interaction and detect of tetragonal phase structure which analysed by TPR and XRD, respectively. The Ni-Co/CeO_2 catalyst showed lower performance in terms of phenol conversion (96.4% at 800 °C) than the Ni-Co/ZrO_2 catalyst. Previous studies of ethanol steam reforming highlighted that the lower level of activity of CeO_2 compared to ZrO_2 is because of the catalyst deactivation by coke formation on the CeO_2-supported catalyst's surface [91]. On the other hand, the Ni-Co/La_2O_3 catalyst produced the minimum conversion of phenol, which was 92% at 800 °C. This is despite that the reducibility and basicity tests showed that it had maximum H_2 consumption and the second highest basic site. The highest surface area, high acidity, and basic sites were achieved for irreducible γ–Al_2O_3 and α–Al_2O_3-supported catalysts, but these two catalysts have lower levels of activity in terms of phenol conversion.

Fig. 7 shows the hydrogen yield of phenol steam reforming in the temperature range of 500 °C to 800 °C. The H_2 yield followed a behaviour that is similar to the phenol conversion. It can be remarked that the entire hydrogen yield increased as the temperature for all supported catalysts increased. The lowest H_2 yield was about 19.8% for Ni-Co/γ-Al_2O_3 at 500 °C, but the temperature increased slightly and reached 85.6% at 800 °C. The Ni-Co/La_2O_3 catalyst had the lowest activity in terms of hydrogen production at high temperatures. This is probably due to the low surface area and the acidity of the Ni-Co/La_2O_3 catalyst. On the other hand, the Ni-Co/α-Al_2O_3 catalyst was more active and presented higher hydrogen formation 500 °C. Clearly, irreducible α-Al_2O_3 oxide support for Ni-Co bimetallic catalyst exhibits higher activity in terms of phenol conversion and hydrogen production at 500–700 °C than the Ni-Co/γ-Al_2O_3, Ni-Co/La_2O_3 and Ni-Co/CeO_2 catalysts. This might be because of the highest acidity of the Ni-Co/α-Al_2O_3 catalyst. The H_2 yield for Ni-Co/α-Al_2O_3 catalyst was 57.6% at 500 °C and increased to 83.5% at 800 °C. This follows previous research which discussed that the alumina support is favoured in a water gas shift reaction, but the disadvantage of this support is that, during dehydration reactions, the deactivation of catalysts by coke formation is caused [92]. Moreover, the Ni-Co/γ-Al_2O_3 catalyst shows high selectivity in terms of extracting hydrogen from phenol. The polymerisation of phenol to coke takes place on both strong acid sites on the Ni-Co/γ-Al_2O_3 catalyst. This results in the formation of polynuclear hydrocarbons, which remain strongly adsorbed on acidic sites and cause loss in activity or form coke multi-layers that lead to cat-

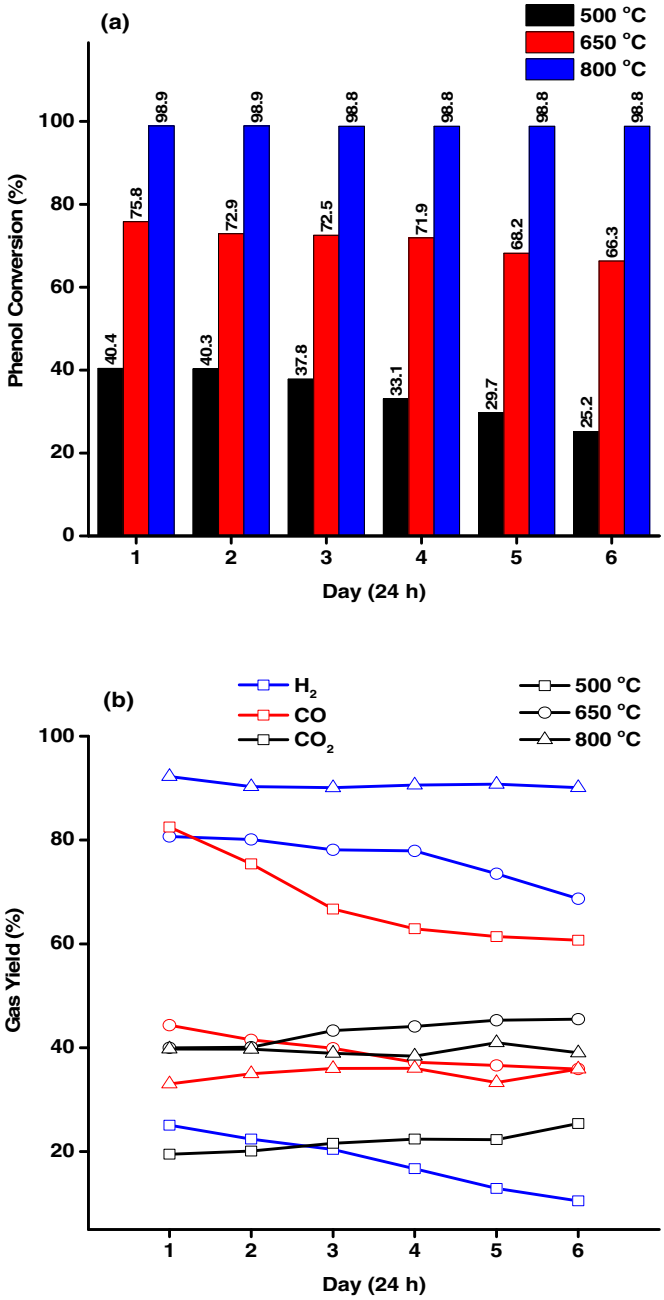

Fig. 8. (a) catalyst staibility based on gas product yield and (b) catalyst staibility based on phenol conversion for ZrO_2 supported catalyst at 500, 650 and 800 °C for 6 days.

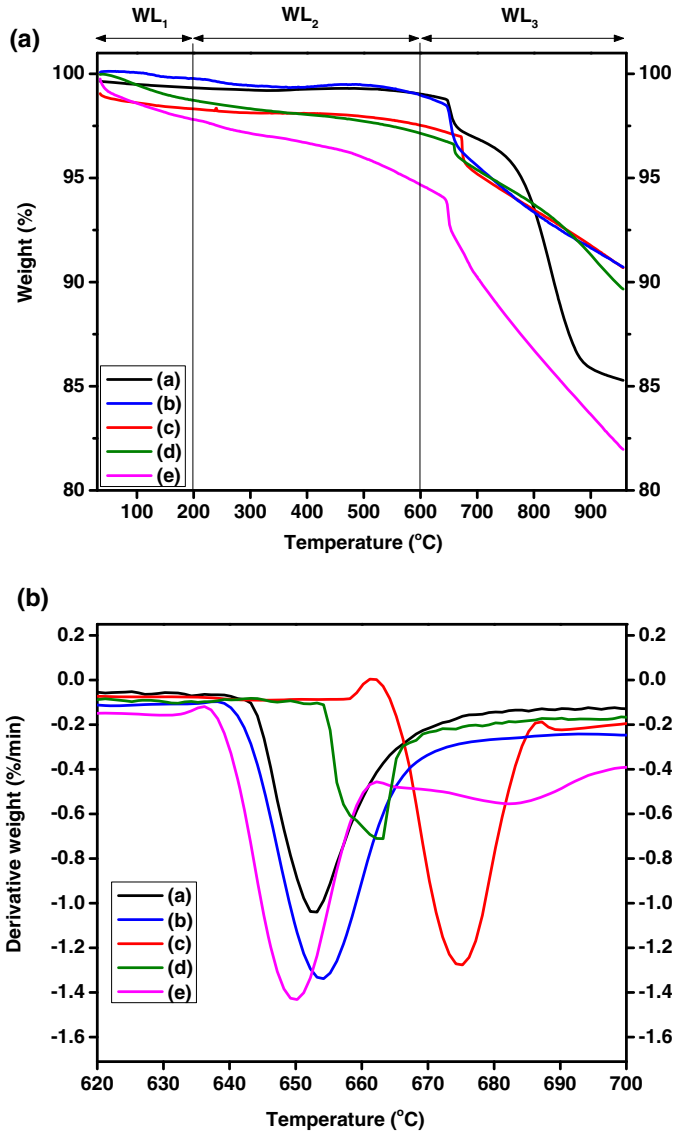

Fig. 9. (a) TGA– (b) DTA curves after 6 h steam reforming for (a) Ni-Co/La_2O_3, (b) Ni-Co/ZrO_2, (c) Ni-Co/CeO_2, (d) Ni-Co/α-Al_2O_3 and (e) Ni-Co/γ-Al_2O_3 catalysts.

Table 2
Weight loss and amount of coke formation on the spent catalysts.

Catalysts	Weight loss (%)			Total weight loss (%)
	WL_1	WL_2	WL_3	
Ni-Co/La_2O_3	0.66	0.31	13.7	14.7
Ni-Co/ZrO_2	0.23	0.8	8.14	9.1
Ni-Co/CeO_2	1.68	0.79	6.7	9.2
Ni-Co/α-Al_2O_3	1.27	1.58	7.3	10.2
Ni-Co/γ-Al_2O_3	2.2	3.13	12.5	17.8

alyst poisoning [61]. These results indicate the choice of support for active metals was very effective for increasing the H_2 yield of phenol conversion. In summary, Ni-Co/ZrO_2 catalyst was more effective in terms of the phenol conversion with higher level of hydrogen selectivity and is selected as promising catalyst.

According to Fig. 6 and Fig. 7, the highest level of activity for phenol steam reforming is found in the Ni-Co/ZrO_2 catalyst. Thus, Ni-Co/ZrO_2 is selected as a promising catalyst for phenol steam reforming in this work. The stability tests of the Ni-Co/ZrO_2 catalyst were performed at 500, 650 and 800 °C, at 0.36 mL/min, and at an atmospheric pressure for 144 h (six days) to investigate the catalyst deactivation phenomenon. Fig. 8 shows the long-term stability measurements of Ni-Co/ZrO_2 in terms of the steam reforming of phenol. It can be clearly seen that at low temperatures such as 500 and 650 °C, the catalyst performance towards phenol conversion and hydrogen yield was gradually decreased by time. The hydrogen yield at 800 °C was constant (92.2%–90.1%) up to 144 h and the phenol conversion changed from 98.91% to 98.87% during this time. However, it can be seen that no deactivation was observed during the 144 h' stability of the Ni-Co/ZrO_2 catalyst at high temperatures.

The carbon content of the spent catalysts was analysed by thermo-gravimetric analyses (TGA) for six hours' time-on-stream of phenol steam reforming reaction and is presented in Fig. 9. Table 2 shows the quantification of weight loss and the amount of carbon deposits during the phenol steam reforming for reducible (CeO_2 and ZrO_2) and irreducible (La_2O_3, γ-Al_2O_3, and α-Al_2O_3)

Table 3
Reaction rate at 800 °C and apparent activation energies (Ea).

Catalyst	Reaction rate (mmol/g s)	Slope	Ea (J/mol)
Ni-Co/La_2O_3	10.40	−6.08	50.57
Ni-Co/ZrO_2	11.17	−12.32	102.41
Ni-Co/CeO_2	10.87	−8.10	67.38
Ni-Co/α-Al_2O_3	10.95	−6.14	51.01
Ni-Co/γ-Al_2O_3	11.02	−9.03	75.07

oxides supports for bimetallic Ni-Co catalysts. In literature, the weight loss region below 200 °C (WL_1) has been attributed to the water and moisture evaporation. The weight loss between 200 and 600 °C (WL_2) has been ascribed to less stable deposits [93], whereas the weight loss above 600 °C (WL_3) is generally attributive to decomposition of coke deposits with more stable [93] and/or different degree of graphitization [94]. In overall, the reducible supports for bimetallic Ni-Co are stronger against coke deposition on their surface than irreducible oxides. The results of the carbon deposition on the catalysts' surfaces showed that the Ni-Co/ZrO_2 catalyst had the lowest level of coking activity while the Ni-Co/γ–Al_2O_3 catalyst showed the highest level of coking among the five tested catalysts. As seen in Fig. 9a and data in Table 2, from the region WL_1, the maximum water and moisture were adsorb on Ni-Co/α-Al_2O_3 catalyst surface (2.2%). The strongest catalyst against the water and moisture adsorption was Ni-Co/ZrO_2 (0.24%). Ni-Co/ZrO_2 catalyst was also the strongest catalyst in WL_2 and WL_2 region with lowest coke deposition on its surface (9.28% of weight loss). For Ni-Co/La_2O_3 and Ni-Co/γ–Al_2O_3 catalysts, the carbon content of the spent catalysts shows 14.7% and 17.8% weight decreased, respectively. This carbon formation has resulted minimum phenol conversion of the Ni-Co/La_2O_3 catalyst compared to other catalysts. However, the results show that Ni-Co/ZrO_2, Ni-Co/α-Al_2O_3, and Ni-Co/CeO_2 catalysts have low carbon deposition. It is illustrated that carbon began to be decomposed at 500 °C and their peaks increased along with the temperature increase. Fig. 9b illustrates the derivative weight loss curves (DTA), which indicate decomposition peaks at 650 °C, 660 °C, and 675 °C. The peaks that are higher than 550 °C represent the decomposition of coke deposits with different degrees of graphite [94]. Jeffery et al. [42] indicated that the use of nitrogen instead of air in the TGA analysis cause to increase material decomposition temperature.

4. Reaction rate and activation energy

The rate of the reaction is a subject of broad importance. It is important in understanding reactions, and has practical implications, too. In our study, the reaction rate of the Ni-Co/La_2O_3, Ni-Co/ZrO_2, Ni-Co/CeO_2, Ni-Co/α-Al_2O_3 and Ni-Co/γ-Al_2O_3 catalysts as function of phenol conversion for each catalyst in the temperature range of 500–800 °C was studied. The rate of reaction ($-r_{Ph}$) based on catalyst weight were calculated from the conversion-residence time kinetic data. It is depicted by Eq. (5).

$$-r_{Ph} = \frac{x_{Ph} Q_{Ph}}{W_{cat}} \quad (5)$$

In this equation, $-r_{Ph}$ is the reaction rate in mmol/g s, x_{Ph} is the conversion of phenol, Q_{Ph} is the flow rate of phenol in mmol/s and W_{cat} is the weight of catalyst in g. The calculated data of the rate model does not include the water concentration because the concentration of water was present in excess compared to the concentration of phenol. The similar assumption was reported for the steam reforming of glycerol [95] and ethanol [96]. The data of the reaction rate are shown in Table 3, this data is in agreement with the catalyst activity tests for phenol conversion. The maximum reaction rate found to be 11.17 mmol/g s with respect to Ni-Co/ZrO_2 catalyst.

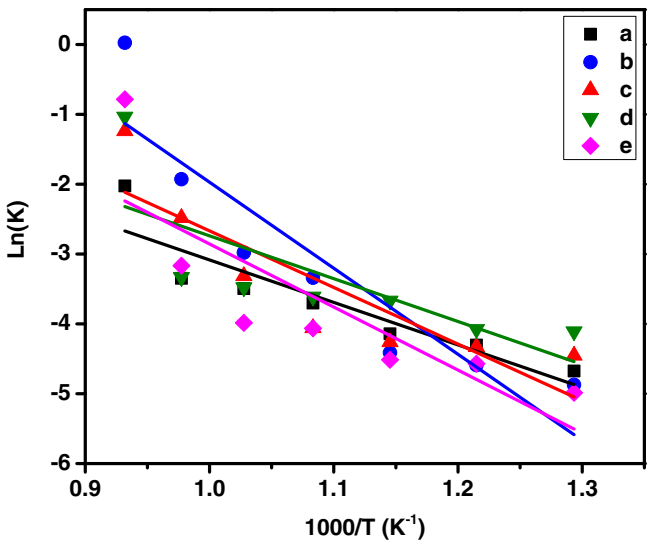

Fig. 10. Arrhenius plot for phenol steam reforming reaction over (a) Ni-Co/La_2O_3, (b) Ni-Co/ZrO_2, (c) Ni-Co/CeO_2, (d) Ni-Co/α-Al_2O_3 and (e) Ni-Co/γ-Al_2O_3 catalysts in the temperature range of 500–800 °C (0.2 g catalyst and 0.36 mL/min feed flow rate).

4.1. Apparent activation energy and comparison of activity

The apparent activation energies were calculated over temperature range of 500–800 °C, based on the phenol conversion. The experimental data were taken after 6 h time-on-stream (TOS) to ensure stable performance of the catalyst. The Arrhenius plots, through which activation energies (E_{app}) were calculated using Eq. (6), are given in Fig. 10. The apparent activation energies were determined from the slopes of the Arrhenius plots.

$$Ln(k) = Ln(A) - \frac{E_A}{RT} \quad (6)$$

where A is pre-exponential factor or frequency factor, E_A is the activation energy (J/mol), R is gas constant (8.314 J/mol K) and T is absolute temperature (K). As it shown in Table 3, it may readily be observed from the slopes that the activation energy of phenol conversion for Ni-Co/ZrO_2 catalyst is comparable and considerably higher than that of other four catalysts.

5. Conclusion

This study investigated hydrogen production as a result of phenol steam reforming using a bimetallic Ni-Co catalyst over two kind of supports such as ZrO_2, CeO_2 (reducible) and La_2O_3, γ-Al_2O_3, and α-Al_2O_3 (irreducible). The characterisation analysis shows that the highest acidity and the largest surface areas were achieved for Ni-Co/γ-Al_2O_3 and Ni-Co/α-Al_2O_3 catalysts. These two supports have the lower levels of activity in terms of phenol conversion and H_2 production than Ni-Co/ZrO_2 catalyst. This is due to coke formation on their surfaces, which results in the deactivation of the catalyst. The Ni-Co/La_2O_3 catalyst showed the low level of phenol conversion and activity for the H_2 yield, which is due to the surface area and high coke formation in its surface. In this work, the Ni-Co/ZrO_2 catalyst illustrated the highest level of activity in terms of phenol conversion (75.9%) at 650 °C. By using this reducible support for bimetallic Ni-Co catalyst, large surface area, strong interaction of metal-support, formation of tetragonal phase of ZrO_2, high acidic site, strong resistant to coke formation, and long-term sta-

bility were achieved. The reaction rate and the activation energy of phenol conversion with respect to Ni-Co/ZrO_2 catalyst were 11.17 mmol/g s and 102.41 (J/mol), respectively.

Acknowledgements

The authors acknowledge the financial support given for this work by Universiti Teknologi Malaysia (UTM) under the Research University Grant (10H19 and 13H36), Flagship 03G10 and The Malaysian Ministry of Higher Education under FRGS 4F403.

References

[1] B. Nabgan, K. Moghadamian, T.A. Tuan Abdullah, W. Nabgan, I. Saeh, Int. J. Environ. Res. Clean Energy 2 (2016) 9–11.
[2] Q. Bu, H. Lei, S. Ren, L. Wang, J. Holladay, Q. Zhang, J. Tang, R. Ruan, Bioresour. Technol. 102 (2011) 7004–7007.
[3] W. Nabgan, I. Saeh, T.A. Tuan Abdullah, B. Nabgan, R. Mat, Y. Gambo, K. Moghadamian, Int. J. Environ. Res. Clean Energy 2 (2016) 1–4.
[4] D.A. Constantinou, A.M. Efstathiou, Appl. Catal. B: Environ. 96 (2010) 276–289.
[5] G. Garbarino, V. Sanchez Escribano, E. Finocchio, G. Busca, Appl. Catal. B: Environ. 113–114 (2012) 281–289.
[6] K. Polychronopoulou, C.N. Costa, A.M. Efstathiou, Catal. Today 112 (2006) 89–93.
[7] K. Polychronopoulou, A. Bakandritsos, V. Tzitzios, J.L.G. Fierro, A.M. Efstathiou, J. Catal. 241 (2006) 132–148.
[8] B. Matas Güell, I.V. Babich, L. Lefferts, K. Seshan, Appl. Catal. B: Environ. 106 (2011) 280–286.
[9] D.A. Constantinou, A.M. Efstathiou, Catal. Today 143 (2009) 17–24.
[10] J.S. Moura, M.O.G. Souza, J.D.A. Bellido, E.M. Assaf, M. Opportus, P. Reyes, M.d.C. Rangel, Int. J. Hydrogen Energy 37 (2012) 3213–3224.
[11] T. de Freitas Silva, J.A.C. Dias, C.G. Maciel, J.M. Assaf, Catal. Sci. Technol. 3 (2013) 635–643.
[12] K. Polychronopoulou, J.L.G. Fierro, A.M. Efstathiou, J. Catal. 228 (2004) 417–432.
[13] D.A. Constantinou, M.C. Álvarez-Galván, J.L.G. Fierro, A.M. Efstathiou, Appl. Catal. B: Environ. 117–118 (2012) 81–95.
[14] D.A. Constantinou, J.L.G. Fierro, A.M. Efstathiou, Appl. Catal. B: Environ. 90 (2009) 347–359.
[15] C. Rioche, S. Kulkarni, F.C. Meunier, J.P. Breen, R. Burch, Appl. Catal. B: Environ. 61 (2005) 130–139.
[16] X. Bi, P. Wang, H. Jiang, J. Hazard. Mater. 154 (2008) 543–549.
[17] L.a. Garcia, R. French, S. Czernik, E. Chornet, Appl. Catal. A: Gen. 201 (2000) 225–239.
[18] H. Xie, J. Lu, M. Shekhar, J.W. Elam, W.N. Delgass, F.H. Ribeiro, E. Weitz, K.R. Poeppelmeier, ACS Catal. 3 (2013) 61–73.
[19] W. Li, Z. Zhao, F. Ding, X. Guo, G. Wang, ACS Sustain. Chem. Eng. 3 (2015) 3461–3476.
[20] S. Shukla, S. Seal, J. Phys. Chem. B 108 (2004) 3395–3399.
[21] K.K. Pant, P. Mohanty, S. Agarwal, A.K. Dalai, Catal. Today 207 (2013) 36–43.
[22] A.C. Basagiannis, X.E. Verykios, Appl. Catal. A: Gen. 308 (2006) 182–193.
[23] L.P.R. Profeti, J.A.C. Dias, J.M. Assaf, E.M. Assaf, J. Power Sources 190 (2009) 525–533.
[24] J.A. Torres, J. Llorca, A. Casanovas, M. Domínguez, J. Salvadó, D. Montané, J. Power Sources 169 (2007) 158–166.
[25] X.-x. Zheng, C.-f. Yan, R.-r. Hu, J. Li, H. Hai, W.-m. Luo, C.-q. Guo, W.-b. Li, Z.-y. Zhou, Int. J. Hydrogen Energy 37 (2012) 12987–12993.
[26] P.G.M. Assaf, F.G.E. Nogueira, E.M. Assaf, Catal. Today 213 (2013) 2–8.
[27] X. Hu, G. Lu, Catal. Commun. 12 (2010) 50–53.
[28] J. Llorca, N.s. Homs, J. Sales, J. Catal. 209 (2002) 306–317.
[29] M.S. Batista, R.K.S. Santos, E.M. Assaf, J.M. Assaf, E.A. Ticianelli, J. Power Sources 134 (2004) 27–32.
[30] E. Papadopoulou, D. Delimaris, A. Denis, A. Machocki, T. Ioannides, Int. J. Hydrogen Energy 37 (2012) 16375–16381.
[31] W. Nabgan, T.A.T. Abdullah, R. Mat, B. Nabgan, A.A. Jalil, L. Firmansyah, S. Triwahyono, Int. J. Hydrogen Energy (2016) 3, http://dx.doi.org/10.1016/j.ijhydene.2016.04.176 [In press].
[32] W. Nabgan, T.A. Tuan Abdullah, R. Mat, B. Nabgan, Y. Gambo, K. Moghadamian, J. Environ. Chem. Eng. 4 (2016) 2765–2773.
[33] J. Zhang, H. Wang, A.K. Dalai, Appl. Catal. A: Gen. 339 (2008) 121–129.
[34] F.F. de Sousa, H.S.A. de Sousa, A.C. Oliveira, M.C.C. Junior, A.P. Ayala, E.B. Barros, B.C. Viana, J.M. Filho, A.C. Oliveira, Int. J. Hydrogen Energy 37 (2012) 3201–3212.
[35] X. Li, J. Ai, W. Li, D. Li, Front. Chem. Eng. China 4 (2010) 476–480.
[36] T.A.T. Abdullah, W. Nabgan, M.J. Kamaruddin, R. Mat, A. Johari, A. Ahmad, Appl. Mech. Mater. 493 (2014) 39–44.
[37] J. Kugai, S. Velu, C. Song, Catal. Lett. 101 (2005) 255–264.
[38] W. Nabgan, T. Tuan Abdullah, R. Mat, B. Nabgan, Y. Gambo, A. Johari, Appl. Sci. 6 (2016) 223.
[39] M.N. Barroso, M.F. Gomez, L.A. Arrúa, M.C. Abello, Catal. Lett. 109 (2006) 13–19.
[40] C. Diagne, H. Idriss, K. Pearson, M.A. Gómez-García, A. Kiennemann, C.R. Chim. 7 (2004) 617–622.
[41] J.B. James, Y.S. Lin, J. Phys. Chem. C 120 (2016) 14015–14026.
[42] J.D. Peterson, S. Vyazovkin, C.A. Wight, Macromol. Chem. Phys. 202 (2001) 775–784.
[43] R.J. Berger, J. Pérez-Ramíırez, F. Kapteijn, J.A. Moulijn, Chem. Eng. Sci. 57 (2002) 4921–4932.
[44] R.K. Irani, B.D. Kulkarni, L.K. Doralswamy, Ind. Eng. Chem. Process Des. Dev. 18 (1979) 648–652.
[45] W. Nabgan, T.A. Tuan Abdullah, R. Mat, B. Nabgan, U.A. Asli, A. Johari, Jurnal Teknologi 78 (2016) 77–82.
[46] S. Hwang, R. Smith, Chem. Eng. Sci. 59 (2004) 4229–4243.
[47] L. Zhao, T. Han, H. Wang, L. Zhang, Y. Liu, Appl. Catal. B: Environ. (2016).
[48] J. Xu, W. Zhou, Z. Li, J. Wang, J. Ma, Int. J. Hydrogen Energy 34 (2009) 6646–6654.
[49] M. Cabo, S. Garroni, E. Pellicer, C. Milanese, A. Girella, A. Marini, E. Rossinyol, S. Suriñach, M.D. Baró, Int. J. Hydrogen Energy 36 (2011) 5400–5410.
[50] S.J. Han, Y. Bang, J. Yoo, J.G. Seo, I.K. Song, Int. J. Hydrogen Energy 38 (2013) 8285–8292.
[51] S.S.Y. Lin, D.H. Kim, S.Y. Ha, Appl. Catal. A: Gen. 355 (2009) 69–77.
[52] G. Zhang, S. Zhang, L. Yang, Z. Zou, D. Zeng, C. Xie, Sens. Actuators B 188 (2013) 137–146.
[53] P. Fleming, R.A. Farrell, J.D. Holmes, M.A. Morris, J. Am. Ceram. Soc. 93 (2010) 1187–1194.
[54] K. Sutthiumporn, S. Kawi, Int. J. Hydrogen Energy 36 (2011) 14435–14446.
[55] Z. Yang, Y. Huang, B. Dong, H.-L. Li, J. Solid State Chem. 178 (2005) 1157–1164.
[56] X. Yang, S. Li, Y. Liu, X. Wei, Y. Liu, J. Power Sources 196 (2011) 4992–4995.
[57] T. Mondal, K.K. Pant, A.K. Dalai, Int. J. Hydrogen Energy 40 (2015) 2529–2544.
[58] M.A. Alves-Rosa, L. Martins, P. Hammer, S.H. Pulcinelli, C.V. Santilli, RSC Adv. 6 (2016) 6686–6694.
[59] M. Rezaei, S.M. Alavi, S. Sahebdelfar, Z.-F. Yan, Mater. Lett. 61 (2007) 2628–2631.
[60] P. Osorio-Vargas, N.A. Flores-González, R.M. Navarro, J.L.G. Fierro, C.H. Campos, P. Reyes, Catal. Today 259 (Part 1) (2015) 27–38.
[61] P. Osorio-Vargas, C.H. Campos, R.M. Navarro, J.L.G. Fierro, P. Reyes, J. Mol. Catal. A: Chem. 407 (2015) 169–181.
[62] F. Aupretre, C. Descorme, D. Duprez, D. Casanave, D. Uzio, J. Catal. 233 (2005) 464–477.
[63] N. Bayat, M. Rezaei, F. Meshkani, Int. J. Hydrogen Energy (2016).
[64] A. Bharadwaj, Y.-P. Ting, Bioresour. Technol. 130 (2013) 673–680.
[65] P.R. Buchireddy, R.M. Bricka, J. Rodriguez, W. Holmes, Energy Fuels 24 (2010) 2707–2715.
[66] L. Wang, D. Li, M. Koike, H. Watanabe, Y. Xu, Y. Nakagawa, K. Tomishige, Fuel 112 (2013) 654–661.
[67] Z. Wang, C. Wang, S. Chen, Y. Liu, Int. J. Hydrogen Energy 39 (2014) 5644–5652.
[68] V. García, J.J. Fernández, W. Ruíz, F. Mondragón, A. Moreno, Catal. Commun. 11 (2009) 240–246.
[69] W. Zheng, J. Zhang, Q. Ge, H. Xu, W. Li, Appl. Catal. B: Environ. 80 (2008) 98–105.
[70] L. Yermán, N. Homs, P. Ramírez de la Piscina, Int. J. Hydrogen Energy 37 (2012) 7094–7100.
[71] S.C. Dantas, J.C. Escritori, R.R. Soares, C.E. Hori, Chem. Eng. J. 156 (2010) 380–387.
[72] G. Sadanandam, K. Ramya, D.B. Kishore, V. Durgakumari, M. Subrahmanyam, K.V.R. Chary, RSC Adv. 4 (2014) 32429–32437.
[73] Y. Wei, H. Wang, K. Li, X. Zhu, Y. Du, J. Rare Earths 28 (2010) 357–361.
[74] J.A. Marrero-Jerez, I.S. Murugan, P. Metcalfe Núñez, Ceram. Int. 40 (2014) 15175–15182.
[75] X. Zhao, G. Lu, Int. J. Hydrogen Energy 41 (5) (2016) 3349–3362.
[76] D. Bazin, L. Borkó, Z. Koppány, I. Kovács, G. Stefler, L.I. Sajó, Z. Schay, L. Guczi, Catal. Lett. 84 (2002) 169–182.
[77] Y. Zhang, Z. Liu, S. Ren, W. Wang, B. Shen, Appl. Catal. A: Gen. 473 (2014) 125–131.
[78] D. Corradini, E. Eksteen, R. Eksteen, P. Schoenmakers, N. Miller, Handbook of HPLC, CRC Press, 2011.
[79] L.P. Bevy, New Developments in Catalysis Research, Nova Science Publishers, 2005.
[80] D. Marani, C. Gadea, J. Hjelm, P. Hjalmarsson, M. Wandel, R. Kiebach, J. Eur. Ceram. Soc. 35 (2015) 1495–1504.
[81] T. Zhang, W. Li, J.-P. Croué, Environ. Sci. Technol. 45 (2011) 9339–9346.
[82] C. Niu, K. Shepherd, D. Martini, J. Tong, J.A. Kelber, D.R. Jennison, A. Bogicevic, Surf. Sci. 465 (2000) 163–176.
[83] E.I. Gürbüz, E.L. Kunkes, J.A. Dumesic, Appl. Catal. B: Environ. 94 (2010) 134–141.
[84] M.M. Natile, A. Glisenti, J. Mol. Catal. A: Chem. 217 (2004) 175–184.
[85] L. Mo, X. Zheng, Q. Jing, H. Lou, J. Fei, Energy Fuels 19 (2005) 49–53.
[86] C.S. Chen, J.H. Lin, J.H. You, K.H. Yang, J. Phys. Chem. A 114 (2009) 3773–3781.
[87] A. Boréave, A. Auroux, C. Guimon, Microporous Mater. 11 (1997) 275–291.
[88] Y. Yang, C. Ochoa-Hernández, V.A. de la Peña O'Shea, P. Pizarro, J.M. Coronado, D.P. Serrano, Appl. Catal. B: Environ. 145 (2014) 91–100.
[89] H. N., High temperature, high pressure hydrocarbon conversion process, 1973. Google Patents.
[90] D.A. Constantinou, J.L.G. Fierro, A.M. Efstathiou, Appl. Catal. B: Environ. 95 (2010) 255–269.

[91] V. Palma, C. Ruocco, F. Castaldo, A. Ricca, D. Boettge, Int. J. Hydrogen Energy 40 (2015) 12650–12662.
[92] A.J. Byrd, K.K. Pant, R.B. Gupta, Ind. Eng. Chem. Res. 46 (2007) 3574–3579.
[93] M. Cobo, D. Pieruccini, R. Abello, L. Ariza, L.F. Córdoba, J.A. Conesa, Int. J. Hydrogen Energy 38 (2013) 5580–5593.
[94] S. Natesakhawat, R.B. Watson, X. Wang, U.S. Ozkan, J. Catal. 234 (2005) 496–508.
[95] S. Adhikari, S.D. Fernando, A. Haryanto, Chem. Eng. Technol. 32 (2009) 541–547.
[96] A. Akande, A. Aboudheir, R. Idem, A. Dalai, Int. J. Hydrogen Energy 31 (2006) 1707–1715.